Thermal noise and the stability of single sonoluminescing bubbles

Ursula H. Augsdörfer,* Allan K. Evans,† and David P. Oxley
Faculty of Computing Science and Engineering, Department of Mathematical Sciences, Institute of Simulation Sciences, De Montfort University, Leicester LE1 9BH, England

(Received 3 November 1999; revised manuscript received 12 January 2000)

The stability of a bubble levitated in an acoustic field under single bubble sonoluminescence conditions was numerically investigated taking thermal noise effects into consideration. Due to the microscopic size of a sonoluminescing bubble thermal noise is important to its surface and is found to cause small irregularities in its spherical shape. A stochastic differential equation in Langevin form is derived to describe the dynamics of a perturbation from the spherical and solved together with the Rayleigh-Plesset equation. The mechanisms responsible for the amplification of small irregularities are examined and a stability threshold is derived, which is in good agreement with experimental threshold data of Holt and Gaitan.

PACS number(s): 78.60.Mq, 47.20.Ma

I. INTRODUCTION

The emission of light by gas bubbles in a liquid excited by ultrasound was first reported in 1933 by Marinesco and Trillat [1]. The phenomenon known as sonoluminescence (SL), was thought to be associated with the transient collapse of cavitating bubbles. In 1989 Gaitan *et al.* [2] discovered the conditions under which a single bubble (SB) can be stably levitated in a standing sound wave and emit light in every cycle of the sound field.

In SBSL the bubble undergoes strong nonlinear oscillations with every cycle of the sound field. The slow expansion and stretching of the bubble surface during the rarefaction phase is followed by a high velocity and almost adiabatic collapse of the bubble to a minimum radius which is determined by the high pressure of the bubble's contents. At this point the contraction reverses and the bubble wall accelerates outward. After the collapse the bubble oscillates around its ambient radius with diminishing amplitude until the next rarefaction phase of the driving sound. For a fixed equilibrium radius R_0 the bubble will during these oscillations, if they are small, exhibit its fundamental resonance frequency ω_0 but large oscillations will have a slightly different frequency because of the nonlinearity of the bubble dynamics.

Observations of unstable bubbles show that they retain their spherical symmetry during the expansion phase, but become unstable after the collapse [3]. Experiments by Holt and Gaitan [4] showed that the stable SBSL regime is defined by the radius of the bubble at ambient pressure R_0 and the amplitude P_a of the driving acoustic pressure $P_d(t) = P_a \cos \omega_s t$, where $\omega_s/2\pi$ is the frequency of the driving sound. As the amplitude P_a of the driving pressure is increased distortions in the bubble's surface lead to its disruption [4].

A theoretical analysis of the bubble's stability will enable us to make a statement about regions in the P_a-R_0 parameter plane at which stable SBSL experiments will be possible. Recent studies on the stability problem are either based on simplifications which have important influence on the result [5,6] or map out a stability threshold for driving pressures which lie well below those applied in SBSL experiments [7,8]. The subject of this paper is to improve the stability analysis by adding corrections to existing models and focus on the stability behavior of bubbles within the P_a-R_0 parameter region.

Distortions from the spherical may be described by superimposing surface spherical harmonics Y_n^m on the mean radius $R(t)$ such that

$$R_{\text{distorted}}(t) = R(t) + \sum_{n=2}^{\infty} \sum_{m=-n}^{n} a_n^m(t) Y_n^m(\theta, \varphi), \quad (1.1)$$

where a_n^m is the distortion amplitude. The superscript m denotes the degree of the spherical harmonics, while its subscript n indicates its mode. Since spherical harmonics are defined by means of Legendre polynomials $Y_n^m(\theta, \varphi) = P_n^m(\theta)\cos(m\varphi)$, it is clear that the wavelength of the shape deformation decreases with increasing mode. For the same amplitude a_n^m, a short wavelength deformation causes a greater increase in the bubble's surface area than a long wavelength deformation. Because surface tension inhibits increases in surface area high-n, short wavelength deformations tend to develop smaller amplitudes than small-n deformations.

The magnitude of each mode n of the shape distortion depends on the dynamics of its amplitude a_n^m. A small amplitude approximation, where it is assumed that $|a_n^m/R| \ll 1$ allows us to describe the dynamics of the distortion amplitude by a linearized differential equation. In this linear approximation the a_n^m's are uncoupled and their dynamics can be approximated by an equation which is independent of the degree m of the spherical harmonic [9–11]. After simplifications (see next section for details) the equation describing the dynamics of the distortion has the form of a damped linear harmonic oscillator

$$\ddot{a}_n(t) + B(t)\dot{a}_n(t) + A(t)a_n(t) = 0. \quad (1.2)$$

*Electronic address: uha@dmu.ac.uk
†Electronic address: ake@dmu.ac.uk

The majority of previous numerical studies [12,13] on the stability problem are based on analyzing whether initial interface distortions of small amplitude grow or diminish with time, where it is assumed that the spherical surface of the bubble is displaced from equilibrium and released at time $t=0$. However, during a sound cycle the stability of a bubble surface is not only affected by its nonlinear motion which may amplify initial perturbations from the spherical, but also exposed to the continual motion of molecules in the surrounding gas and liquid. Molecular fluctuations are more important for bubbles on the microscopic scale typical for SBSL bubbles.

The present stability investigation was stimulated by the work of Brenner *et al.* [5] and Hilgenfeldt *et al.* [6] who first considered the effects of thermal fluctuation in their analysis, but adds a significant correction to the physical model. Molecular fluctuations within the bubble and the surrounding liquid act as a random force on the bubble surface. Therefore, this investigation will improve upon earlier models by introducing a random force to the dynamics of the distortion amplitude rather than a random displacement. Prosperetti and Hao [7] extended the stability model by introducing a nonzero right-hand side in the stability equation (1.2), but did not give a definite expression. The present analysis clarifies the remaining problem of the expression on the nonzero right-hand side of Eq. (1.2). Using the equipartition theorem and the theory of Langevin equations, we derive the correct form of this expression and examine its consequences for a bubble in the SL parameter region. In this paper we also treat the flow of heat into and out of the bubble, improving on the adiabatic or isothermal approximations used by other authors [5,6,14].

II. DYNAMICS OF THE DISTORTION AMPLITUDE

The equation of motion for distortions of amplitude, a_n, for a stationary bubble in a viscous fluid was first derived by Prosperetti [11]. Due to the problem of distribution of vorticity which is determined by the prior motion of the free surface, this equation has integrodifferential structure and its numerical solution is a difficult task. Several ways of simplification have since been applied: the complexity of Prosperetti's equation can be significantly reduced if it is assumed that vorticity has no time to spread into the liquid so that its effects can be ignored. This is the most common approximation to the stability problem and frequently applied when the surface stability of a gas bubble in liquid is discussed [3,11,15].

In order to simplify the problem with a higher degree of accuracy Prosperetti [16], Hilgenfeldt *et al.* [6], and Brenner *et al.* [5] applied a boundary-layer approximation to the problem, where it is assumed that vorticity spreads only into a small boundary layer around the bubble. Hilgenfeldt *et al.* [6] and Brenner *et al.* [5] in their approach additionally modified the original derived equation of the boundary-layer approximation by means of a Taylor expansion, which leads to a damping term very much smaller than in the original approximation.

All authors [3,5–7,11,15,16] treat the problem assuming that the viscosity and density of the gas are negligible. However, density effects may become important at the end of a violent collapse, where the compressed gas has a density comparable to that of the surrounding liquid. In this analysis we therefore consider the dynamics of the gas inside the bubble, but, to keep the problem tractable, ignore its viscosity as in previous simulations.

If, as in Refs. [16,6], it is assumed that vorticity spreads out only into a small liquid boundary layer of size δ around the bubble and one neglects only the viscosity of the gas, the equation of motion as derived by Prosperetti [11] can be simplified to Eq. (1.2), where expressions $A(t)$ and $B(t)$ have the form

$$B(t)=\frac{3\dot{R}}{R}+2\frac{\eta_l}{\zeta R^2}\left(-\beta+\frac{n^2(n+2)^2}{1+2\delta/R}\right), \tag{2.1}$$

$$A(t)=[(n+1)(n+2)\rho_g-n(n-1)\rho_l]\frac{\ddot{R}}{\zeta R}+\frac{\beta\sigma}{\zeta R^3}$$
$$+\frac{2\eta_l}{\zeta}\frac{\dot{R}}{R^3}\left(\beta-\frac{n^2(n-1)(n+2)}{1+2\delta/R}\right), \tag{2.2}$$

where $\beta=n(n-1)(n+1)(n+2)$ and $\zeta=n\rho_l+\rho_g(n+1)$. $R,\dot{R},\ddot{R}$ denote the radius, velocity, and acceleration of the bubble wall, ρ_l, σ, and η_l refer to the density, surface tension, and viscosity of the surrounding liquid, and ρ_g is the density of the gas inside the bubble.

Prosperetti and Hao [16], Brenner *et al.* [5], and Hilgenfeldt *et al.* [6] approximate the boundary layer thickness δ by the diffusive length scale $\sqrt{\nu_l\tau}$, where $\nu_l=\eta_l/\rho_l$ is the kinematic viscosity of the liquid. As a time scale they choose $\tau=1/\omega_s$, where $\omega_s/(2\pi)$ is the frequency of the driving sound field. To prevent the boundary layer around a small bubble from growing larger than the radius of the bubble itself we determine the width of the boundary layer by the cutoff criteria introduced by Brenner *et al.* [5] and Hilgenfeldt *et al.* [6] according to which

$$\delta=\min\left(\sqrt{\frac{\nu_l}{\omega_s}},\frac{R(t)}{2n}\right). \tag{2.3}$$

III. ADDING A THERMAL NOISE TERM

Molecular fluctuations in the surroundings of the bubble wall act as a random force on the bubble surface. To model the effect of this random force on the dynamics of the distortion, the ordinary differential equation (1.2) which determines its dynamics has to be rewritten in the form of a stochastic differential equation

$$\ddot{a}_n(t)+B(t)\dot{a}_n(t)+A(t)a_n(t)=C(t)f(t), \tag{3.1}$$

where $f(t)$ denotes the temporally uncorrelated random force simulated as white Gaussian noise with unit variance. We first consider the case where $A(t)=A$, $B(t)=B$, and $C(t)=C$ are constants independent of t. Using standard methods [17] it can be shown that the root mean square amplitude a_n of the deformation is given by

$$\sqrt{\langle a_n^2\rangle}=\frac{\sqrt{2AB}}{C}. \tag{3.2}$$

The equipartition theorem [18] also implies (see the Appendix) that at equilibrium

$$\sqrt{\langle a_n^2 \rangle} = \left(\frac{kT_0}{\sigma(n^2+n+2)} \right)^{1/2}, \tag{3.3}$$

with k representing the Boltzmann constant and T_0 the equilibrium temperature. We therefore set

$$C = \left(\frac{2kT_0 AB}{\sigma(n^2+n+2)} \right)^{1/2} \tag{3.4}$$

effectively choosing the amplitude of the fluctuations to satisfy the equipartition theorem. We now make the assumption that the timescale for molecular fluctuations is much shorter than that of the bubble motion. This is clearly true, because a bubble with surface area 10^{-9} m^2 experiences on the order of 10^{21} molecular collisions per second from a gas at atmospheric pressure. Thus, we can assume Eq. (3.4) will give the correct amplitude for thermal noise even when A and B depend on time. This formula is therefore used in our numerical simulations.

According to a recent analysis of thermal conduction effects in SL [19] the temperature at the bubble wall is most of the cycle close to the ambient liquid temperature, due to the formation of a cold, dense layer of air at the bubble wall during its contraction. As the bubble hits its minimum radius the temperature is predicted to change for only a few nanoseconds. According to the fluctuation dissipation theorem [20] the time required for thermal noise to affect the dynamics of a system corresponds to the damping time of the system. The damping time for bubble shape oscillations is of the order of microseconds. It is thus reasonable to apply the equilibrium formula to SL bubbles. In water at room temperature and in equilibrium the amplitude of surface deformations caused by thermal noise will have an amplitude of about 80 pm for small n.

From Eq. (3.3) it is evident that the size of the deformation due to noise effects decreases with increasing mode n of the deformation. In addition, keeping the expression of spherical harmonics in terms of Legendre polynomials in mind, the forcing required to excite modes increases with the mode number. We will discuss therefore in the following only the low distortion-mode components.

IV. RADIAL MOTION

To describe the bubble's motion in the sound field we refer to the Keller-Miksis model accounting to first order for the liquid compressibility [21], given by

$$\left(1-\frac{\dot{R}}{c_l}\right)\ddot{R}R+\frac{3}{2}\left(1-\frac{\dot{R}}{3c_l}\right)\dot{R}^2 = \left(\frac{1}{\rho_l}+\frac{\dot{R}}{\rho_l c_l}\right)(P_b-P_\infty)+\frac{R}{\rho_l c_l}\frac{d}{dt}(P_b-P_\infty), \tag{4.1}$$

where P_b is the pressure on the liquid side of the bubble wall given by

$$P_b = P_g - \frac{2\sigma}{R} - \frac{4\eta_l}{R}\dot{R}. \tag{4.2}$$

$R, \dot{R}, \ddot{R}$ denote the bubble radius, the velocity of the bubble wall, and its acceleration, ρ_l, η_l, and σ refer to density, viscosity, and surface tension of the surrounding liquid, respectively and c_l denotes the speed of sound in the liquid. To describe the pressure of the gas P_g inside the bubble we apply the van der Waals equation of state. Neglecting attractive forces between the molecules has no effect on the physics discussed here, and we can use the van der Waals equation in the simplified form

$$P_g(t) = \frac{\mathcal{N}\Re T_g(t)}{V(t)-b}, \tag{4.3}$$

where $\mathcal{N}$ is the number of moles present in the bubble, $\Re$ is the universal gas constant, T_g is the bubble's internal temperature, V is the volume of the bubble, and b is the excluded van der Waals hard core volume.

An equation to determine the temperature dynamics of the gas inside the bubble was derived from the first law of thermodynamics,

$$\frac{dU(t)}{dt} = \frac{dQ(t)}{dt} - P\frac{dV(t)}{dt}, \tag{4.4}$$

where dU denotes the change in internal energy of the system, dQ is the heat added to the system and $P\,dV$ is the work done on the system.

For a perfect gas the internal energy can be expressed in terms of the molar specific heat of the gas at constant volume, C_V, and change in temperature, dT, so that

$$\frac{dU(t)}{dt} = \mathcal{N}C_V\frac{dT(t)}{dt}. \tag{4.5}$$

In the case of a gas bubble the heat absorbed by the gas is given by

$$\frac{dQ(t)}{dt} = \mathcal{N}C_V\frac{T_0-T_g(t)}{\tau}, \tag{4.6}$$

where τ is the thermal diffusion time and T_0 is the temperature of the surrounding fluid.

Substituting Eqs. (4.5) and (4.6) into Eq. (4.4) we find that the temperature of the gas inside the bubble varies with the bubble's volume $V(t)$ as

$$\frac{dT_g(t)}{dt} = \frac{T_0-T_g(t)}{\tau} - \frac{P_g(t)}{\mathcal{N}C_V}\frac{dV(t)}{dt}, \tag{4.7}$$

where P_g is the pressure inside the bubble. We set $\tau = R(t)^2/(\pi^2 D_g)$, which is the relaxation time for exponential decay of the first Fourier mode in the spherically symmetric solution of the heat diffusion equation. D_g denotes the thermal diffusivity of the gas, given by

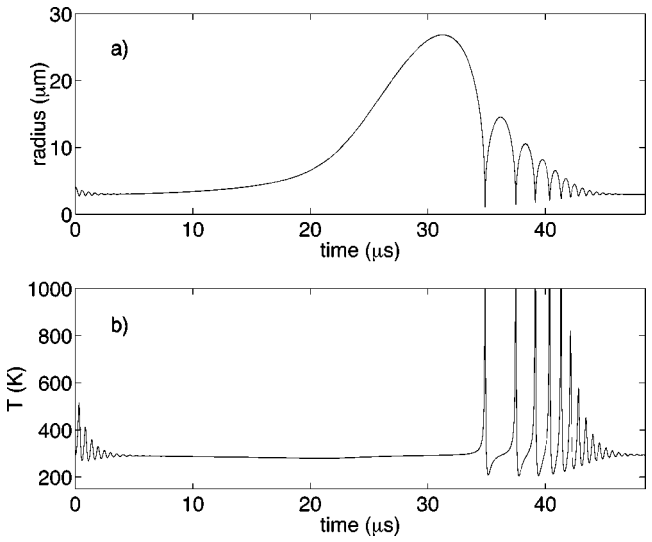

FIG. 1. (a) Radius versus time over one cycle in a sound field with a pressure amplitude of $P_a=1.2$ bar and a radial frequency $\omega_d=2\pi\times 20.6$ kHz. The bubble has an equilibrium radius of $R_0=4$ μm. (b) Corresponding temperature dynamics inside the bubble as a function of time. The maximum temperature occurs at the bubble's minimum radius $R_{\min}=34.8$ μs and reaches about 17 000 K. The maximum temperatures are not displayed to make information at smaller temperatures visible in more detail.

$$D_g=\frac{\kappa_g V}{\mathcal{N}C_P}, \tag{4.8}$$

with C_P denoting the molar specific heat at constant pressure. The coefficient of thermal conductivity κ_g is given by [22]

$$\kappa_g=\frac{1}{3}\lambda_g\overline{v}_g C_V(\mathcal{N}/V)=\frac{2C_V}{3\sigma_g N_A}\left(\frac{kT_g}{\pi m_g}\right)^{1/2}, \tag{4.9}$$

where T_g is the bubbles internal temperature, N_A denotes Avogadro's constant, and m_g, λ_g, σ_g, and $\overline{v}_g$ are the mass, the mean free path, the collision cross section, and the mean speed of a gas molecule, respectively.

A solution to the Keller-Miksis equation of motion together with the van der Waals equation of state coupled with the above equation for the temperature dynamics inside the bubble is shown in Fig. 1. Figure 1(a) is a plot of a bubble's radial dynamics versus time for a bubble with an equilibrium radius $R_0=4$ μm in a sound field with a pressure amplitude $P_a=1.2$ bar. Figure 1(b) is a plot of the corresponding temperature inside the bubble versus time. The maximum temperature at the bubble's minimum radius is about 17 000 K. Introducing the heat conduction to the model improves the agreement with experimental data when compared to an isothermal or adiabatic model. The importance of the energy loss due to heat flow for the stability dynamics has already been pointed out by Prosperetti and Hao [7] who found that when including a thermal damping term the deformation is significantly weakened. A comparison between the thermal damping predicted by the approximation introduced here and the model of Chapman and Plesset [23] shows close agreement.

Recent experiments by Matula and Crum [24] and Ketterling and Apfel [25] confirm a hypothesis by Lohse *et al.* [26] according to which chemical reactions inside the bubble will transform an air bubble to a pure argon bubble. Therefore, all parameters are chosen to represent an argon bubble in water and may be used to interpret air bubble experiments. Constants used in the simulation are given in Table I.

Due to its stochastic character we need to apply a stochastic generalization of standard numerical methods to solve Eq. (3.1). Thus, we will solve Eq. (3.1) together with the Keller-Miksis Eq. (4.1) and Eq. (4.7) using the standard form of Langevin's formula [27].

TABLE I. Constants used in the numerical simulation.

	Sound		
Frequency	$\omega_s/2\pi$	20.6	kHz
Speed in water	c_l	1481	$\mathrm{m\,s^{-1}}$
	water		
Ambient pressure	P_0	1	bar
Ambient temperature	T_0	293.16	K
Viscosity	η_l	10^{-3}	$\mathrm{kg\,m^{-1}\ s^{-1}}$
Density	ρ_l	10^3	$\mathrm{kg\,m^{-3}}$
Surface tension	σ	0.073	$\mathrm{N\,m^{-1}}$
	argon		
Hard core v. d. Waals radius	h	$R_0/8.86$	m
No. of moles per unit volume	N_g	44.67	$\mathrm{m^{-3}}$
Molar heat capacity, const. volume	C_V	12.5	$\mathrm{J\,K^{-1}}$
Molar heat capacity, const. pressure	C_P	20.8	$\mathrm{J\,K^{-1}}$
Mass per mole	M_g	39.9×10^{-3}	kg
Mass per atom	m_g	6.68×10^{-26}	kg
Collision cross section	σ_g	36×10^{-20}	$\mathrm{m^2}$
Viscosity	η_g	21×10^{-6}	$\mathrm{kg\,m^{-1}\ s^{-1}}$

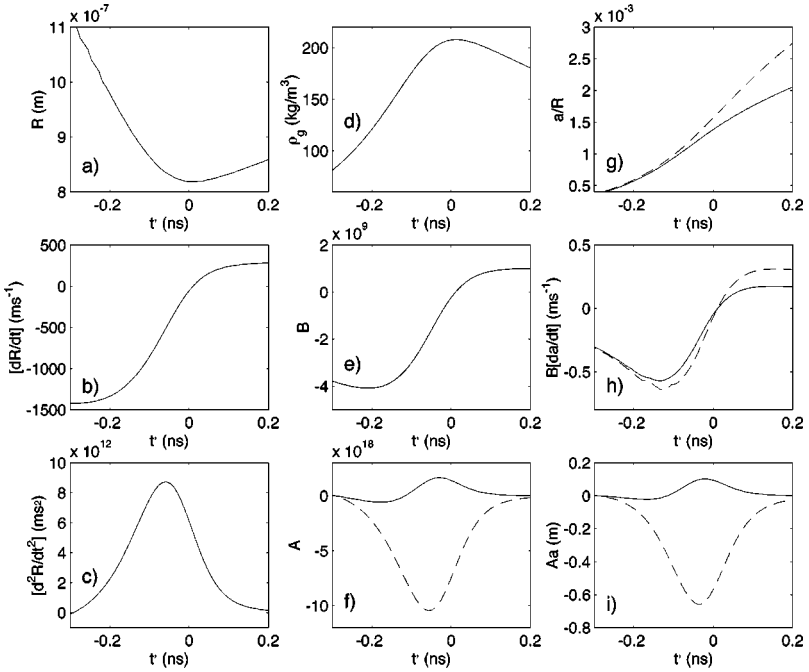

FIG. 2. (a)–(d) The bubble's radius, velocity, acceleration, and gas density respectively, are plotted as a function of time during the final stages of collapse and the turnaround, $R_0=4$ μm, $P_a=1.4$ bar. (e) and (f) show the corresponding dynamics of the dimensionless expressions $B(t)$ and $A(t)$ in Eq. (3.1). Both are shown in comparison with their dynamics (dotted line) in the case where the density of the gas is neglected. While for the damping term $B(t)$ (e) the difference between the solutions is negligible, strong compression may reverse the sign of the term $A(t)$ (f). An example of a typical $(n=2)$ mode deformation (normalized) is plotted in (g). If density is ignored the deformation after the collapse is considerably stronger (dotted line). (h) and (i) show the magnitudes $B(t)\dot{a}_2(t)$ and $A(t)a_2(t)$, respectively.

V. RESULTS AND DISCUSSION

The solution of Eq. (3.1) can be used to describe a number of different instability characteristics, which act not only on different time scales but also in different P_a-R_0 parameter regions. We will distinguish between two types of instability mechanisms responsible for the amplification of small perturbations during one cycle.

The well-known Rayleigh-Taylor [28] instability acts as the bubble wall is strongly accelerated outwards (from the gas into the liquid). The mechanism acts suddenly and on a nanosecond time scale. Although the Rayleigh-Taylor instability amplifies small perturbations caused by molecular fluctuation during one cycle, the mechanism is not strong enough to lead to the bubble's disruption in the parameter region relevant to SL.

The problem of an amplification of deformation caused by the bubble's volume oscillations after the collapse goes back to Faraday [29]. He discovered that a free surface of liquid when oscillating periodically and normal to its surface will induce waves (Faraday waves) on its surface of half the frequency of the oscillation. Longuet-Higgins [30] showed that this also applies to spherical surfaces. For any surface mode n, strong Faraday instability will occur as $2\omega_n/\omega_0$ approaches unity and resonance coupling between surface and volume oscillations occurs. In contrast to Prosperetti and Hao [7], who assigned the development of Faraday waves only to the build-up of instabilities over more than one cycle, we find that maximal deformation due to the Faraday mechanism will develop within microseconds and occurs more than three bounces after the collapse.

Surface waves due to Faraday instability may be responsible for the increase in the signal reflected from the bubble surface a few radial oscillations after the collapse as observed in light-scattering experiments by Matula and Crum [31].

From the characteristics of the Faraday instability it is clear that the resonance frequency ω_0 of the bubble is of vital importance to the stability dynamics. If in the physical model the gas was assumed to behave isothermally its stiffness would be greatly underestimated leading to a comparatively low resonance frequency [32]. As a consequence resonance coupling between radial and modal oscillations, leading to a maximum amplification of surface waves, would occur at larger equilibrium radii. Also important are the damping mechanics of the bubble motion since the bubble's resonance frequency ω_0 will reduce with damping. Additionally, as mentioned above, the amplification of surface waves will be significantly stronger than in the undamped model. It is therefore essential to determine the thermal dynamics of the system, a fact ignored in earlier studies [6,14].

We now consider the effect of the gas density ρ_g on the stability problem. During the collapse of a bubble, but before the final moments of very high compression, the first term $3\dot{R}/R$ in Eq. (2.1) is large and negative. The introduction of ρ_g reduces the size of the second term, but this effect is unimportant because the first term is dominant. A negative value of $B(t)$ leads to instability, and this instability is almost unaffected by the gas density. This is illustrated in Fig. 2(e).

While the damping is not significantly altered during strong collapse, including the gas density has important effects on the coefficient $A(t)$ in Eq. (2.2). When the bubble radius is close to its minimum, the velocity of the bubble wall is small and the acceleration of the gas towards the liquid is very large. In classical stability models, where gas density is neglected, strong Rayleigh-Taylor instability will occur. This is represented in Eq. (3.1) by a large negative value of the coefficient $A(t)$. When gas density is included this Rayleigh-Taylor effect is weakened, as can be seen from Eq. (2.2). For very strong compression, as in the case of small bubbles in strong sound fields, $A(t)$ may even become positive and cause the amplitude of deformations to decrease (see Fig. 2). This, however, is only true at the end of a violent collapse with strong compression. During the subsequent afterbounces Rayleigh-Taylor instability will occur and additionally increase perturbations amplified during a

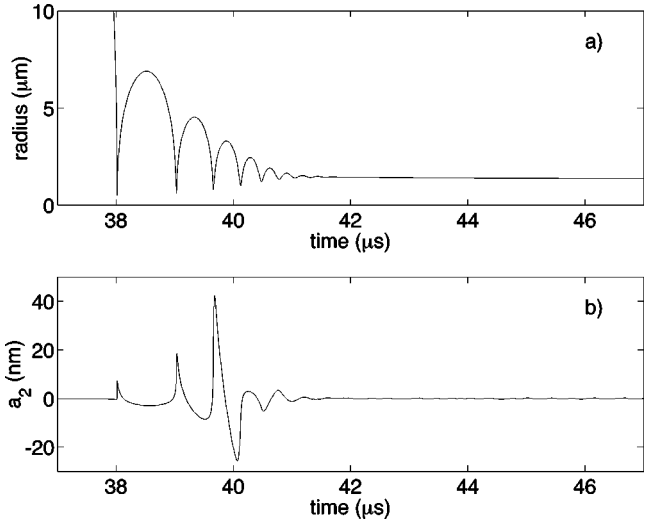

FIG. 3. (a) Radius versus time during the final stages of collapse and the radial bounces following the collapse, $R_0=2$ μm, $P_a=1.4$ bar. (b) Typical corresponding $(n=2)$ mode deformation. After a strong amplification at $t\approx 38.7$ μs due to a violent bubble collapse, perturbations get additionally amplified due to Rayleigh-Taylor instability from secondary minima occurring with further bounces.

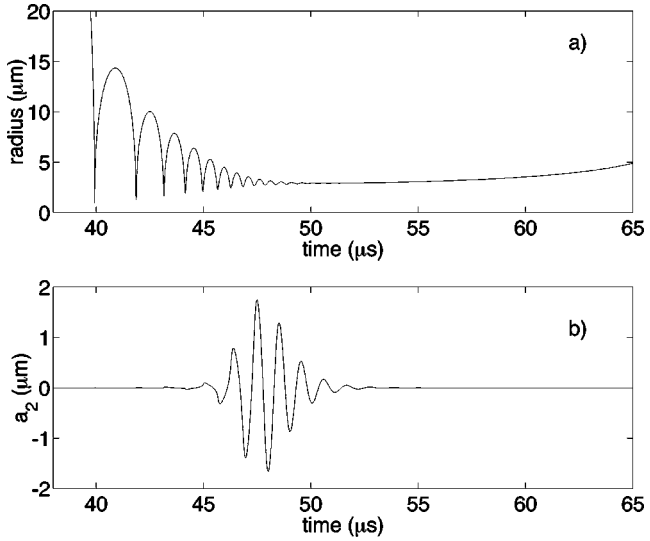

FIG. 4. (a) The bubble radius as a function of time during collapse until the next sound cycle, $R_0=4$ μm, $P_a=1.4$ bar. Below (b) the corresponding amplitude of $(n=2)$ mode deformation, which reaches a maximum seven radial bounces after the bubble reached its first minimum at $t\approx 39.9$ μs.

violent collapse. We will therefore refer to the deformation over the first 2–3 bounces after the collapse as Rayleigh-Taylor instability.

According to Prosperetti and Hao [7] the development of surface deformations during the radial bounces after the collapse is directly related to the Rayleigh-Taylor effect. However, we find that the mechanisms can be separated and act in different parameter regimes. The Rayleigh-Taylor instability is more pronounced for small bubbles which undergo a stronger collapse, while the Faraday instability on the other hand is responsible for the deformation of larger bubbles and may lead to their disruption during one cycle. In particular the bubble shown in Fig. 4 has a maximal deformation $\max|a_2|=16$ nm over the first three bounces as $t<44.5$ μs, while the smaller bubble in Fig. 3 in an equally strong sound field develops a comparably larger deformation during its first three bounces, but no additional amplification occurs and the perturbation will be quickly damped out. Only the larger bubble shown in Fig. 4 is Faraday unstable.

Figure 5 shows the mean maximum normalized perturbation developed during one cycle within the P_a-R_0 parameter plane. The mean was derived from ten different solutions, each obtained using a different string i of random numbers, so that $\langle \max|a_2/R|\rangle=\frac{1}{10}\Sigma_{k=1}^{10}\max|a_2/R|_{i_k}$. In Fig. 5(a) the maximum deformation due to Rayleigh-Taylor instability only is shown. While large bubbles are stable over the first 2–3 bounces after the collapse throughout the range of driving pressures, small bubbles can become Rayleigh-Taylor unstable at higher driving pressures.

The Faraday instability is shown in Fig. 5(b). After a peak, which indicates the equilibrium radius at which resonance coupling between the volume and surface oscillations occurs, the maximum deformation due to Faraday waves will cease. This however, does not imply that the bubble will retain its spherical symmetry for higher radii. Higher modes are excited at higher equilibrium bubble radii. Additionally, coupling between surface modes is becoming important, which is beyond the scope of this analysis.

Both, the Rayleigh-Taylor and Faraday instability amplify small perturbation caused by molecular fluctuation but only the latter is strong enough to amplify surface waves which lead to the bubble's disruption in a single cycle. As an estimate we assume the possible break up of a bubble if in one of ten cycles the size of the deformation reaches the size of the radius $|a_2/R|=1$ as in previous simulations [5–7].

If strong surface waves develop during the after bounces and restoring forces are weak, distortions may not be entirely stretched out during the next expansion phase. As a consequence the deformation developed in the first cycle will experience a second and subsequent amplification in the following cycles. A third instability mechanism, referred to as parametric instability is responsible for the build-up of shape instabilities over more than one cycle. A bubble is assumed to be parametrically unstable if for every one of ten solutions, each obtained with a different string of random numbers to simulate thermal noise, the instability grows from cycle to cycle. For each cycle we used the same string of random numbers.

As shown in Fig. 6 for larger bubbles at driving pressures below SL amplitudes the parametric instability sets in before the bubble's disruption during a single cycle. At near-SL acoustic pressures (about 1.2–1.5 bar), a parametrically stable bubble may get disrupted during one single cycle. An important difference between these two types of instability, which both may lead to the bubble's disruption, is the speed with which the deformation and subsequent disruption occurs. While the deformation during one cycle within the SL parameter range (1 μm$\leqslant R_0\leqslant 7$ μm, 1.2 bar$\leqslant P_a\leqslant 1.4$ bar) never exceeds about 150 m/s, deformation which builds up over several cycles may reach enormous speed ($>10^6$ m/s). One may expect a bubble which disrupts ''slowly'' into a mass of microbubbles to reform at the antinode since the mass of bubbles is not scattered far apart. As

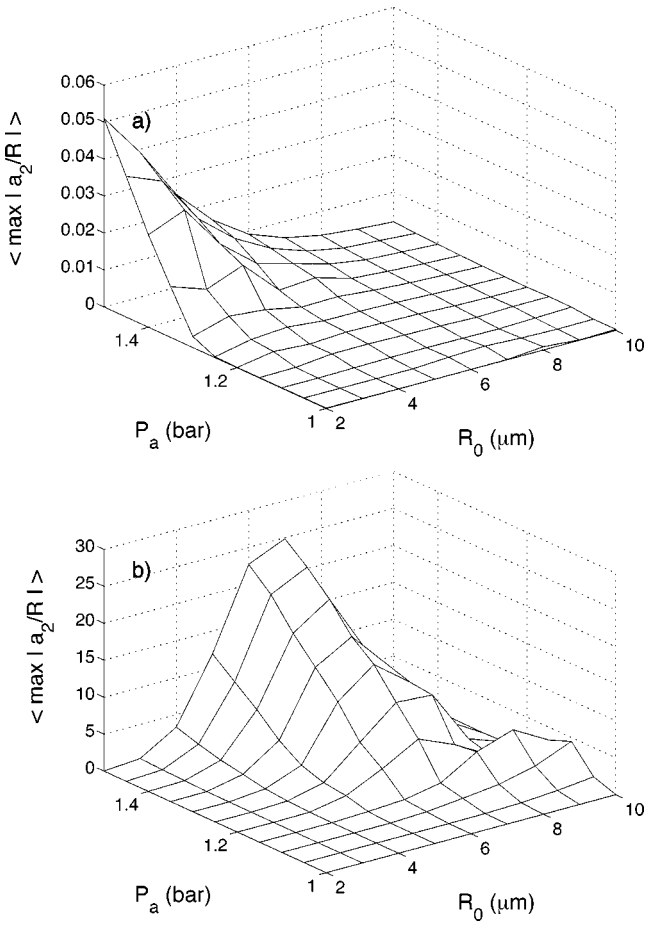

FIG. 5. (a) The mean maximum of the normalized $(n=2)$ deformation during the first three radial bounces after collapse, where Rayleigh-Taylor occurs. The mean is plotted as a function of driving pressure amplitude P_a and the bubbles equilibrium radius R_0. (b) The mean maximum amplitude of normalized surface waves during the bubbles radial bounce, from the third radial bounce after the collapse until the next expansion phase.

a result they may merge at the driving pressure antinode of the sound field as they expand during the next rarefaction phase. This may explain the appearance of bubbles which repeatedly grow, shape oscillate, and break up in the sound field. What is termed ''recycling'' bubbles was observed by Holt and Gaitan [4] at driving pressures between 0.8 and 1.4 bar. In the case of parametric unstable bubbles on the other hand, the final disruption occurs with such a high speed that the resulting micro bubbles will be ejected from the sound field trap which makes a recombination impossible. Thus, the onset of parametric instability defines the extinction threshold in a SBSL experiment, since a bubble beyond this threshold will not survive more than a few cycles.

In Fig. 6 the numerical solution for the onset of the $(n=2)$ and $(n=3)$ mode parametric instability and the threshold above which the bubble may get disrupted by the $(n=2)$ mode during a single sound cycle is compared to experimental threshold data from Holt and Gaitan. We compare the numerical solution not only to data where the mode of the deformation was identified [$\bigcirc$ indicates where bubbles deform in a $(n=2)$ mode manner and $\triangle$ indicates $(n=3)$ mode deformations], but also to recorded unstable bubbles where the mode could not be classified ($\times$). Since we expect

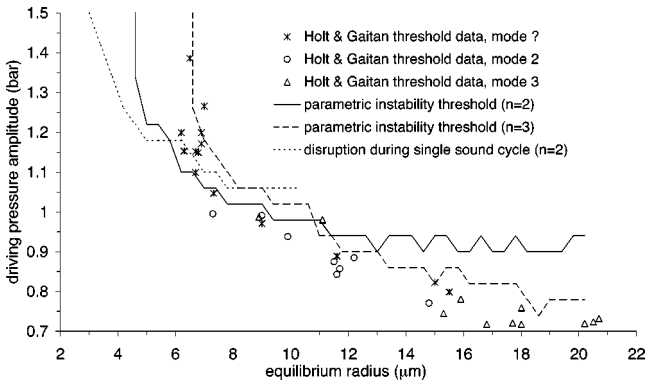

FIG. 6. The numerical derived thresholds for which a bubble is found to be $(n=2)$ mode parametric instable (—), $(n=3)$ mode parametric unstable (– –), and may disrupt by two-mode deformation during a single cycle $(\cdots)$ is plotted within the equilibrium radius, R_0, and the sound pressure amplitude, P_a, parameter plane. Stability threshold data from experiments by Holt and Gaitan are indicated by crosses for instable bubbles where the mode was not identified, by circles for 2-mode instable bubbles, and by triangles for 3-mode instable bubbles.

larger modes to become important only for bubbles larger than in the SBSL regime, it is reasonable to compare these data points to numerical instability thresholds for small mode deformations.

The numerical results show that for bubbles with an equilibrium radius R_0 larger than about 10 μm the $(n=3)$ mode distortion will become parametrical unstable *before* the $(n=2)$ mode parametric instability sets in. This is in close agreement with experiments where for bubbles with $R_0>13$ μm only the $(n=3)$ mode was observed, while the $(n=2)$ mode perturbation dominates for smaller bubbles.

The experimentally obtained $(n=2)$ mode instability threshold indicates a trend for bubbles with $R_0>11$ μm which deviates from the numerical predicted onset of $(n=2)$ mode parametric instability, but instead corresponds well with the onset $(n=3)$ mode parametric threshold. This discrepancy hints that coupling between the distortion modes may occur and the onset of $(n=3)$ instability stimulates the smaller perturbation mode.

For SBSL bubbles, which have smaller equilibrium radii, $R_0 \leqslant 7$ μm, the $(n=2)$ mode distortion must dominate the bubble's surface oscillations. Our numerical solution shows that in this regime a bubble becomes $(n=2)$ mode unstable before $(n=3)$ mode perturbations can be observed either as parametrical instability or for recycling bubbles. We conclude therefore that bubbles disrupting in strong pressure fields ($P_a \geqslant 1.1$ bar) where the distortion mode could not be resolved in experiments by Holt and Gaitan are most likely $(n=2)$ mode unstable.

The comparison shows that the agreement of the numerically determined parametric instability threshold with experimental data is good and clearly marks an improvement to earlier simulations [5–7,14].

VI. CONCLUSION

The stability of the surface of a micron-sized argon bubble in water was analyzed with focus on the sonolumi-

nescence parameter region. We show that molecular fluctuations in the bubble wall neighborhood cause small ripples within the bubble's surface. The equation describing the dynamics of the perturbation amplitude as derived by Prosperetti [11] was simplified by means of a boundary-layer approximation [5,6,16] including density variations inside the bubble which have been neglected in previous studies. The equation is additionally modified to allow for heat flow and thermal noise and rewritten in the form of a stochastic differential equation.

Solving the stochastic differential equation together with the Keller-Miksis equation and an equation describing the temperature dynamics inside the bubble by means of Langevin's formula enabled us to investigate the surface stability of a cavitating bubble under SBSL conditions. Two different mechanisms responsible for the amplification of small perturbations during one cycle are discussed: while Rayleigh-Taylor instability is responsible for the deformation of small bubbles with equilibrium radii smaller than 3 μm in strong sound fields, the Faraday instability causes waves in the surface of larger bubbles. In a boundary-layer approach the latter instability mechanism may lead to the bubble's disruption within one cycle [Fig. 5(b)].

The extinction threshold observed in SBSL experiments by Holt and Gaitan [4,33] and Gaitan and Holt [34] is found to correspond with the onset of parametric instability where amplified deformations built up over more than one cycle (Fig. 6). While including density variations to the stability problem increases the general stability during one cycle of a bubble after the collapse, the onset of parametric instability remains unchanged.

ACKNOWLEDGMENTS

The authors thank G. Holt and W. Moss for valuable comments and G. Holt and F. Gaitan for making their experimental data available.

APPENDIX: SURFACE PERTURBATION AT EQUILIBRIUM

Suppose the bubble's radius is

$$r(\theta,\phi)=R_0+\epsilon P_n^m(\theta)\sin(m\varphi), \tag{A1}$$

where $P_n^m(\theta)$ is an associated Legendre polynomial, and R_0 is the radius of the bubble in spherical equilibrium. Since the area of the surface is given by

$$A=\int_0^{\pi} d\theta \int_0^{2\pi} d\varphi\, r\sin\theta\left[r^2+\left(\frac{\partial r}{\partial\theta}\right)^2+\frac{1}{\sin^2\theta}+\left(\frac{\partial r}{\partial\theta}\right)^2\right]^{1/2}, \tag{A2}$$

one can easily calculate the area to second order in ϵ:

$$A=4\pi R_0^2+\frac{\pi\epsilon^2}{2}\int_0^{\pi} d\theta\sin\theta\left[2[P_n^m(\theta)]^2+\left(\frac{mP_n^m(\theta)}{d\theta}\right)^2+\left(\frac{mP_n^m(\theta)}{\sin\theta}\right)^2\right]+O(\epsilon^3). \tag{A3}$$

Using the standard integrals [35]

$$\int_0^{\pi} d\theta[P_n^m(\theta)]^2\sin\theta=\frac{2}{2n+1}\frac{(n+m)!}{(n-m)!} \tag{A4}$$

and

$$\int_0^{\pi} d\theta\left[\left(\frac{dP_n^m(\theta)}{d\theta}\right)^2+\left(\frac{mP_n^m(\theta)}{\sin\theta}\right)^2\right]\sin\theta=\frac{2n(n+1)}{2n+1}\frac{(n+m)!}{(n-m)!}, \tag{A5}$$

A can be expressed as

$$A=4\pi R_0^2+\pi\epsilon^2\frac{(n^2+n+2)}{(2n+1)}\frac{(n+m)!}{(n-m)!}+O(\epsilon^3). \tag{A6}$$

The surface energy associated with an increase in area δA is simply $\sigma\delta A$, where σ is the surface tension. By setting

$$\frac{kT}{2}=\sigma\delta A, \tag{A7}$$

a root-mean square amplitude ϵ_n^m for each spherical harmonic can be obtained in accordance with the equipartition theorem [18]. The result is

$$(\epsilon_n^m)^2=\frac{kT}{2\pi\sigma}\frac{(2n+1)}{(n^2+n+2)}\frac{(n+m)!}{(n+m)!}. \tag{A8}$$

The functions $Y_n^m(\theta,\phi)=P_n^m(\theta)\cos(m\phi)$ are not normalized. To find a measure of the amplitude of deviations from spherical symmetry, the normalization integral [11] was used to define the amplitude ψ as the root-mean-square deviation, average over the bubble's surface

$$\psi^2=\int_0^{\pi} d\theta\int_0^{2\pi} d\varphi\sin\theta(r-R_0)^2. \tag{A9}$$

For a spherical harmonic deviation with size ϵ_n^m as in Eq. (A8), one simply has

$$\psi=\left(\frac{kT}{\sigma(n^2+n+2)}\right)^{1/2}. \tag{A10}$$

Formula (A10) gives the approximate size of deviations from spherical symmetry for a bubble in equilibrium at constant temperature.

[1] N. Marinesco and J.J. Trillat, C. R. Acad. Sci. URSS, Ser. A **196**, 858 (1933).
[2] D.F. Gaitan, L.A. Crum, C.C. Church, and R.A. Roy, J. Acoust. Soc. Am. **91**, 3166 (1992).
[3] E.A. Neppiras, Phys. Rep. **61**, 159 (1980).
[4] R.G. Holt and D.F. Gaitan, Phys. Rev. Lett. **77**, 3791 (1996).
[5] M.P. Brenner, D. Lohse, and T.F. Dupont, Phys. Rev. Lett. **75**, 954 (1995).
[6] S. Hilgenfeldt, D. Lohse, and M.P. Brenner, Phys. Fluids **8**, 2808 (1996).
[7] A. Prosperetti and Y. Hao, Philos. Trans. R. Soc. London, Ser. A **357**, 203 (1999).
[8] Y. Hao and A. Prosperetti, Phys. Fluids **11**, 1309 (1999).
[9] G. Birkhoff, Q. Appl. Math. **12**, 306 (1954).
[10] M.S. Plesset, J. Appl. Phys. **25**, 96 (1954).
[11] A. Prosperetti, Q. Appl. Math. **34**, 339 (1977).
[12] M. Plesset and T. Mitchell, Q. Appl. Math. **13**, 419 (1956).
[13] R. Chapman and M. Plesset, J. Basic Eng. **94**, 142 (1972).
[14] C.C. Wu and P.H. Roberts, Phys. Lett. A **250**, 131 (1998).
[15] B.P. Barber *et al.*, Phys. Rep. **281**, 65 (1997).
[16] A. Prosperetti, Atti Accad. Naz. Lincei, Cl. Sci. Fis. Mat. Nat. Rend. **LXII**, 196 (1977).
[17] S. Chandrasekhar, *Noise and Stochastic Processes* (Dover, New York, 1954).
[18] L.D. Landau and E.M. Lifshitz, *Statistical Physics*, 3rd ed. (Pergamon, Oxford, 1980), Pt. I.
[19] M.D. Chu and D. Leung, J. Phys.: Condens. Matter **9**, 3387 (1997).
[20] J.R. Waldram, *The Theory of Thermodynamics* (Cambridge University Press, Cambridge, 1985).
[21] A. Prosperetti and A. Lezzi, J. Fluid Mech. **168**, 457 (1986).
[22] P.W. Atkins, *Physical Chemistry*, 2nd ed. (Oxford University Press, Oxford, 1983).
[23] R.B. Chapman and M.S. Plesset, J. Basic Eng. **93**, 373 (1971).
[24] T.J. Matula and L.A. Crum, Phys. Rev. Lett. **80**, 865 (1998).
[25] A. Ketterling and R.E. Apfel, Phys. Rev. Lett. **81**, 4991 (1998).
[26] D. Lohse *et al.*, Phys. Rev. Lett. **78**, 1359 (1997).
[27] D.T. Gillespie, *Markov Processes* (Academic Press, San Diego, 1992).
[28] S.G. Taylor, Proc. R. Soc. London, Ser. A **201**, 192 (1950).
[29] M. Faraday, Philos. Trans. R. Soc. London **121**, 299 (1831).
[30] M.S. Longuet-Higgins, J. Fluid Mech. **201**, 543 (1989).
[31] T.J. Matula and L.A. Crum, in *Proceedings of the 16th International Congress on Acoustics and 135th Meeting Acoustical Society of America*, edited by P.K. Kuhl and L.A. Crum (ASA, Seattle, 1998).
[32] T.G. Leighton, *The Acoustic Bubble* (Academic Press, Cambridge, 1994).
[33] R.G. Holt and D.F. Gaitan, in *Proceedings of the 3rd Microgravity Fluid Physics Conference* (NASA Conference Publications, Cleveland, 1996).
[34] D. F. Gaitan and R. G. Holt, in *Proceedings of the 16th International Congress on Acoustics and 135th Meeting Acoustical Society of America*, edited by P.K. Kuhl and L.A. Crum (ASA, Seattle, 1998).
[35] G. Arfken, *Mathematical Methods for Physicists* (Academic Press, San Diego, 1985).